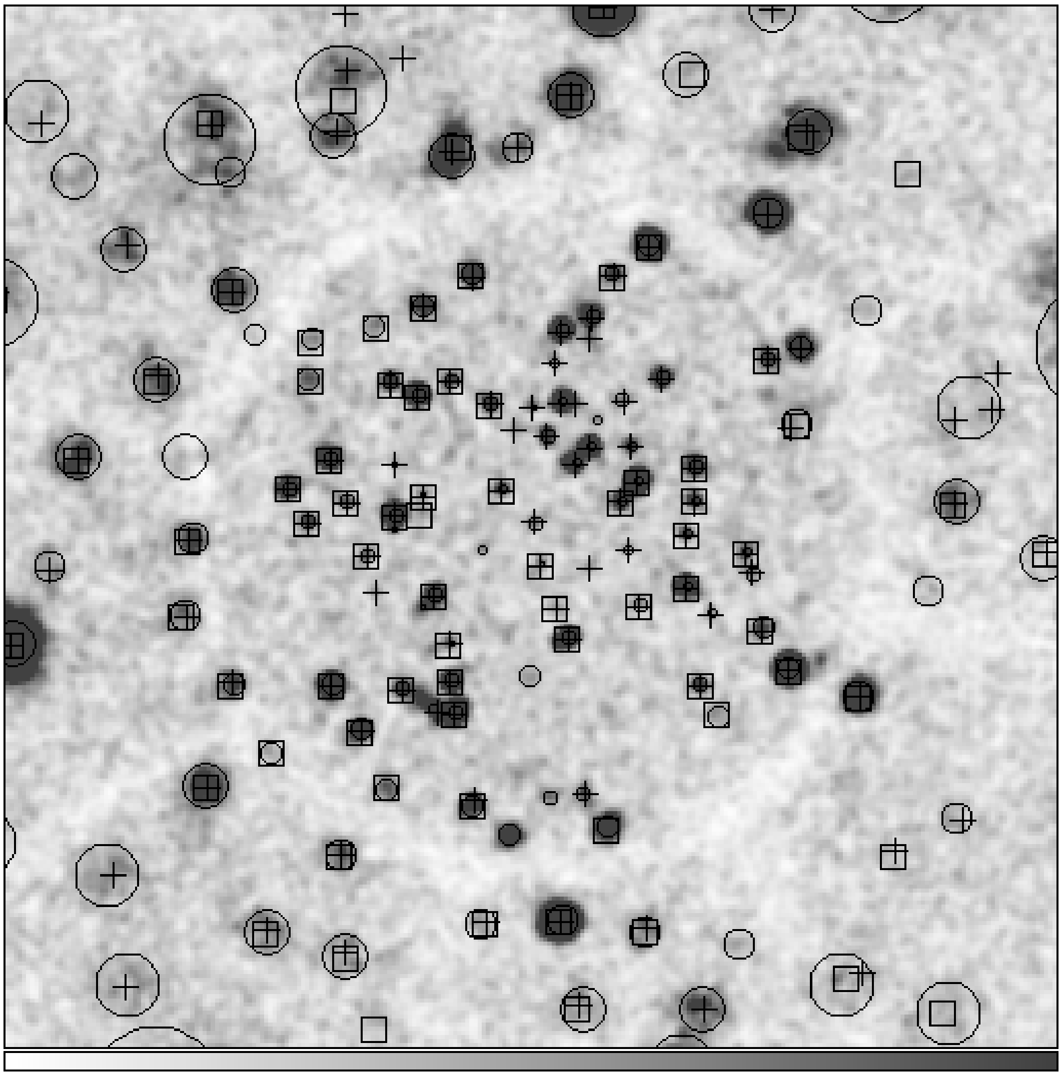

Fig. 12.— Actual PSPC images, used to compare the performances of WT, WGA and MPE methods (north is at the top, and east to the left). The original photon images have been smoothed with a gaussian with $\sigma = 1$ pixel ($15''$). Circles indicate sources detected using WT with significance above 4.2σ, and their radius is equal to the scale a_{max} of highest-significance detection (highest value of $y(a)$). Plus signs are sources from the WGA catalog, and squares sources from the MPE catalog. See the text for details of this comparison. (a): central part (32×32 arcmin) of Pleiades cluster (RP200068): some obvious sources are detected by WT but not by either WGA or MPE, especially close to the ribs. (b): enlargement ($2\times$) of center of Figure 12a: two close pairs of sources are resolved by the WT, but are detected as a single source each by the other methods. (c): full field of view of SN 1987A, in the LMC (RP500100): no WGA sources are available for this region, while MPE misses some obvious emission features, recognized by the WT method. (d): enlargement ($2\times$) of Figure 12c, showing more clearly the complex emission features present in the field. (e): the galaxy NGC 4636 (RP600016), full field of view, and (f) its enlargement ($2\times$): many MPE detections without either a WT or WGA counterpart are spread over the diffuse envelope of this galaxy, and might arise from an underestimate of the local background. In the external regions many WGA detections are found in the direction of the large-scale background gradient. (g): the AGN 1442+101 (RP701002), full field of view, and (h) its enlargement ($2\times$): here again many WGA detections lie in the direction of the large-scale background gradient.

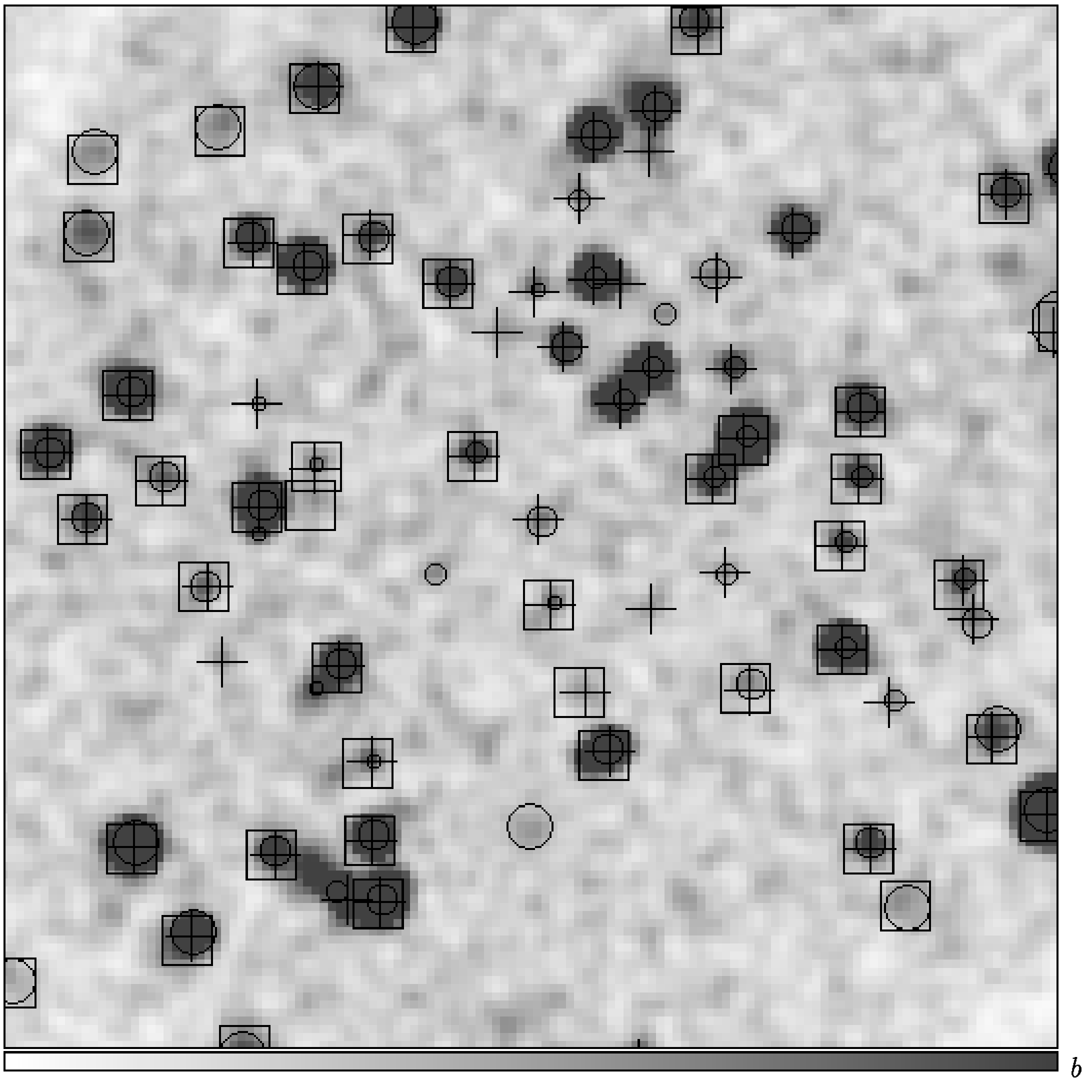

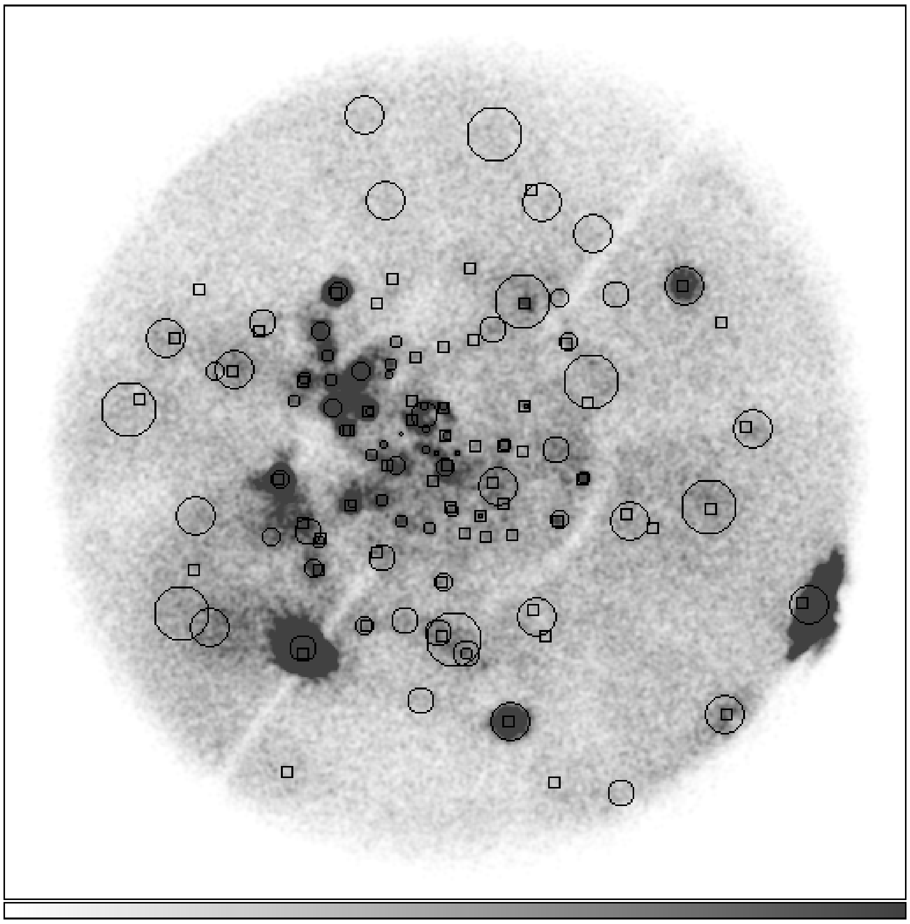

c

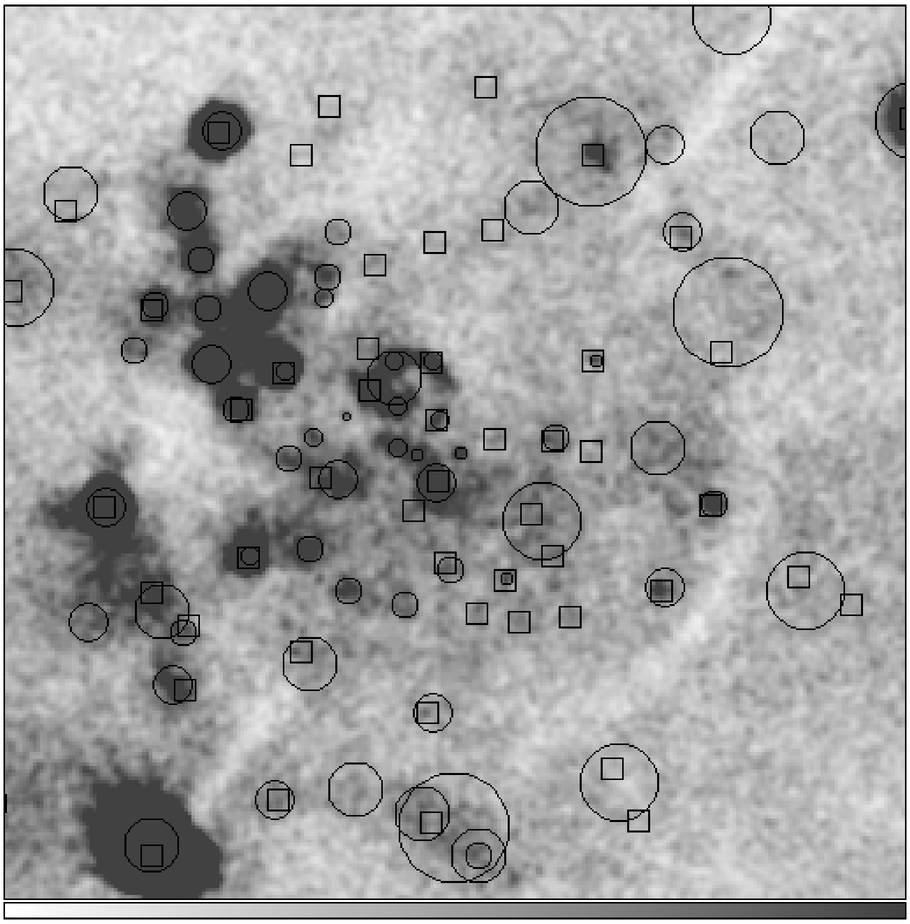

d

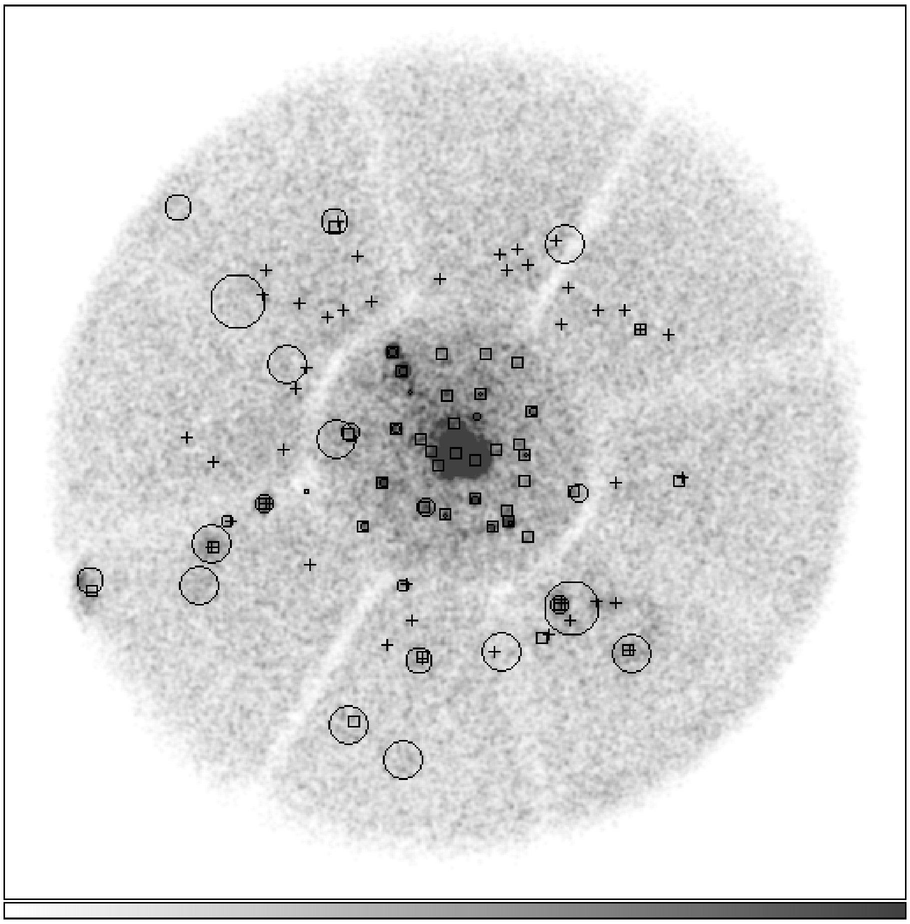

e

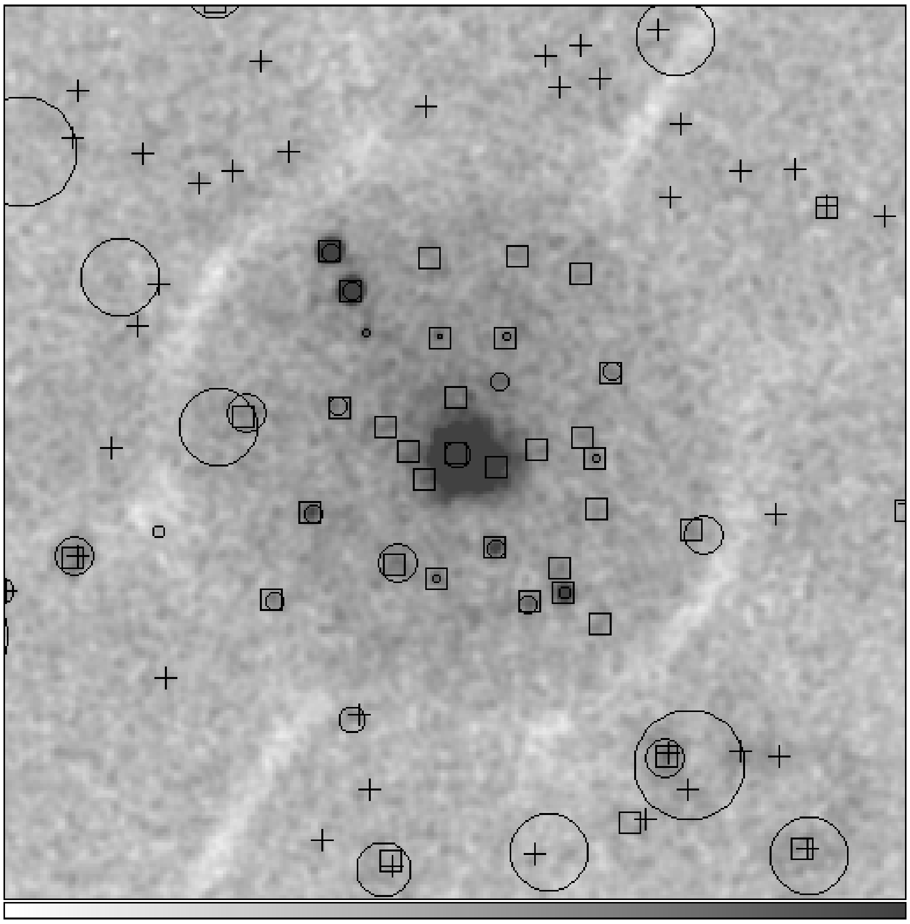

f

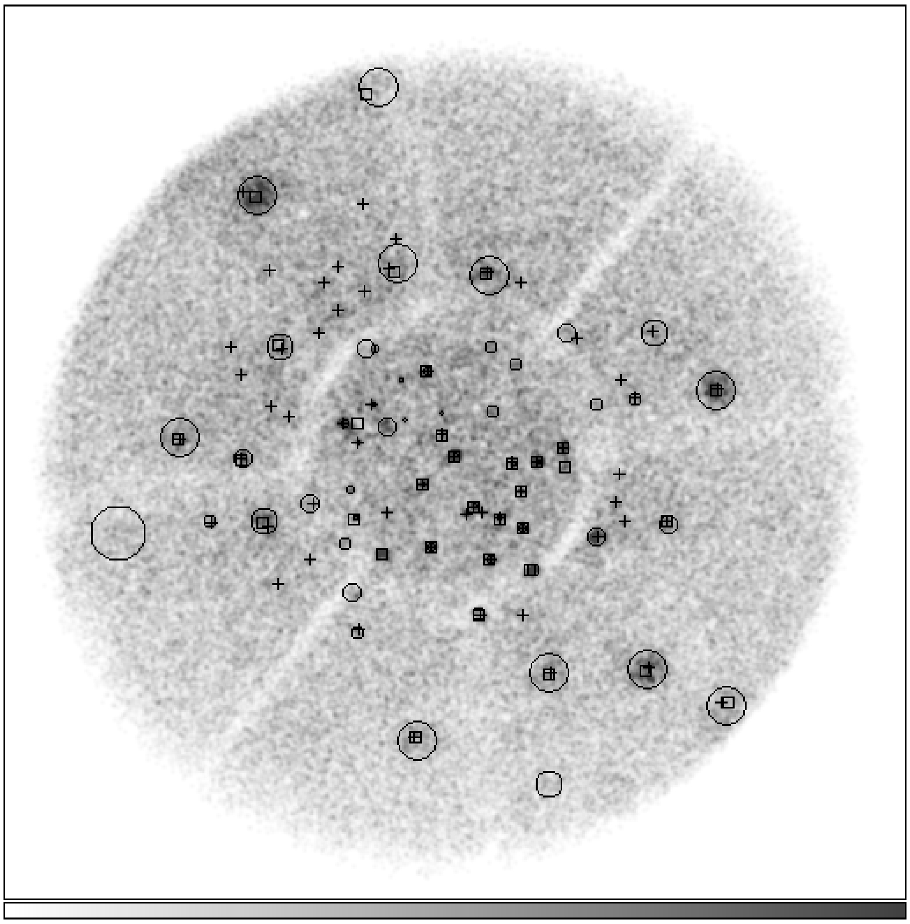

g

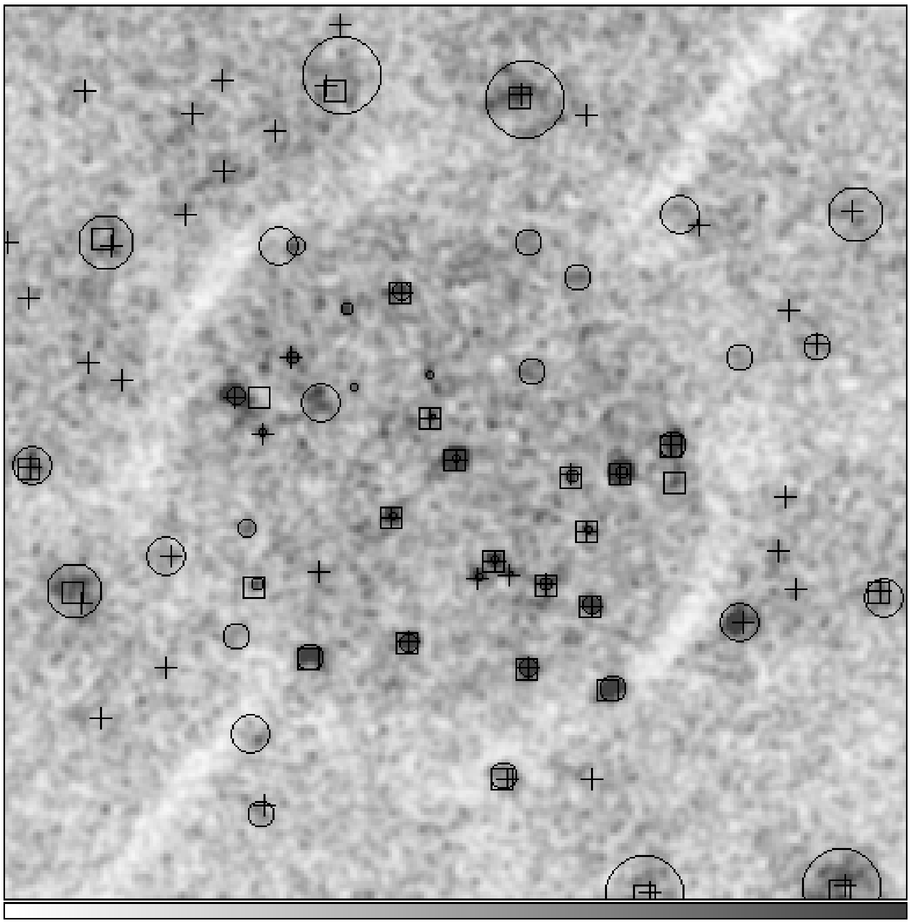

h

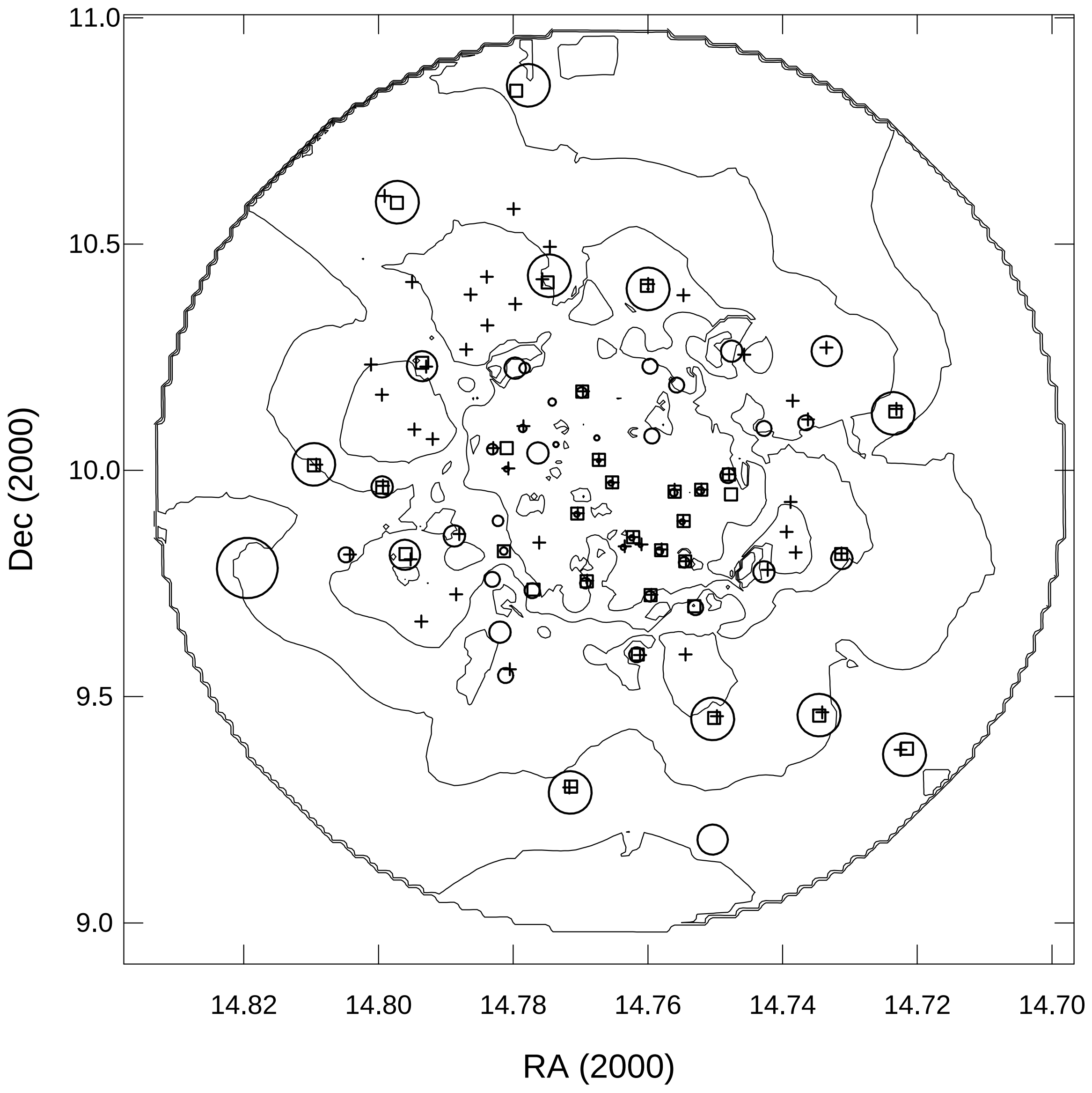

Fig. 13.— Contours of smoothed background, with detected sources removed, for the image RP701002. Sources detected by WT, WGA, and MPE methods, respectively, are indicated with the same symbols of Figure 12. It can be seen that (apart from the vignetting effect) the background has a gradient from SW towards NE, and that many sources detected only by WGA lie precisely in regions of enhanced background emission.

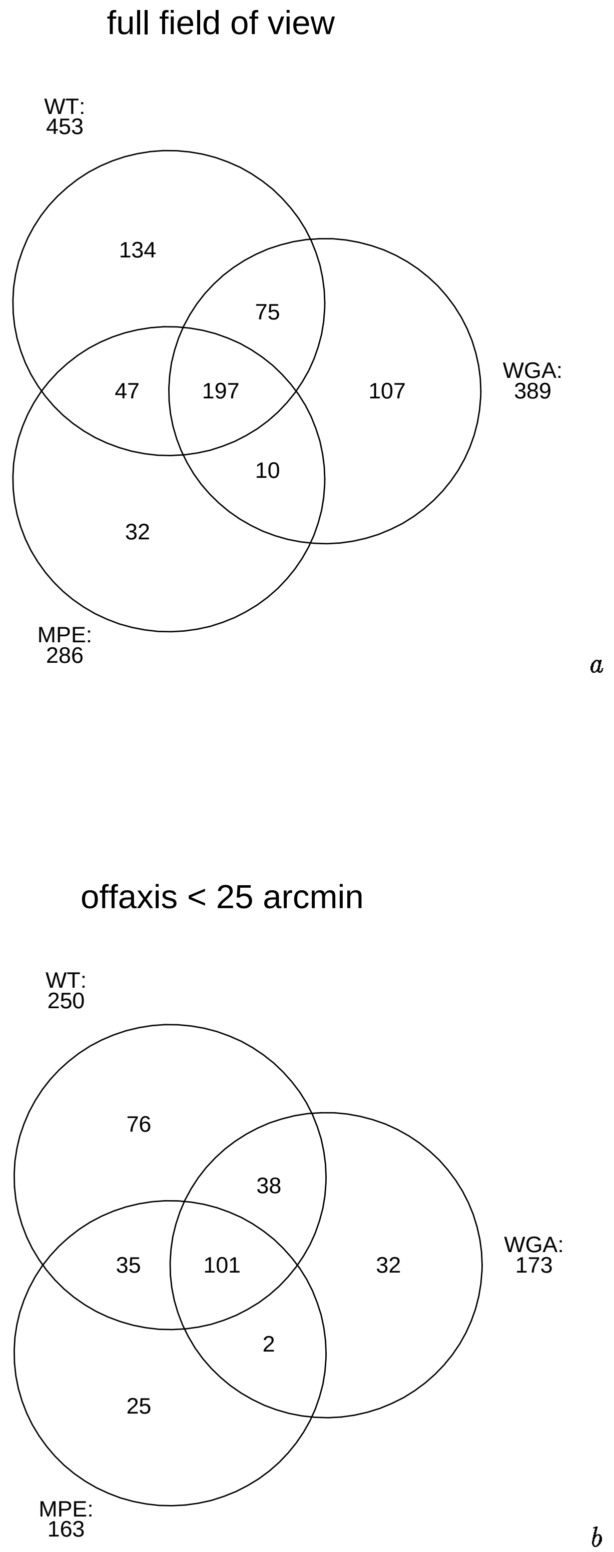

Fig. 14.— Diagram showing the number of sources detected with our method (WT), and extracted from the WGA and MPE catalogs of PSPC sources, respectively, summed on all test images of Table 1, for (*a*) the whole field of view, and (*b*) the central region within 25′ off-axis. Detections common to more than one method fall in the intersection between different circles.

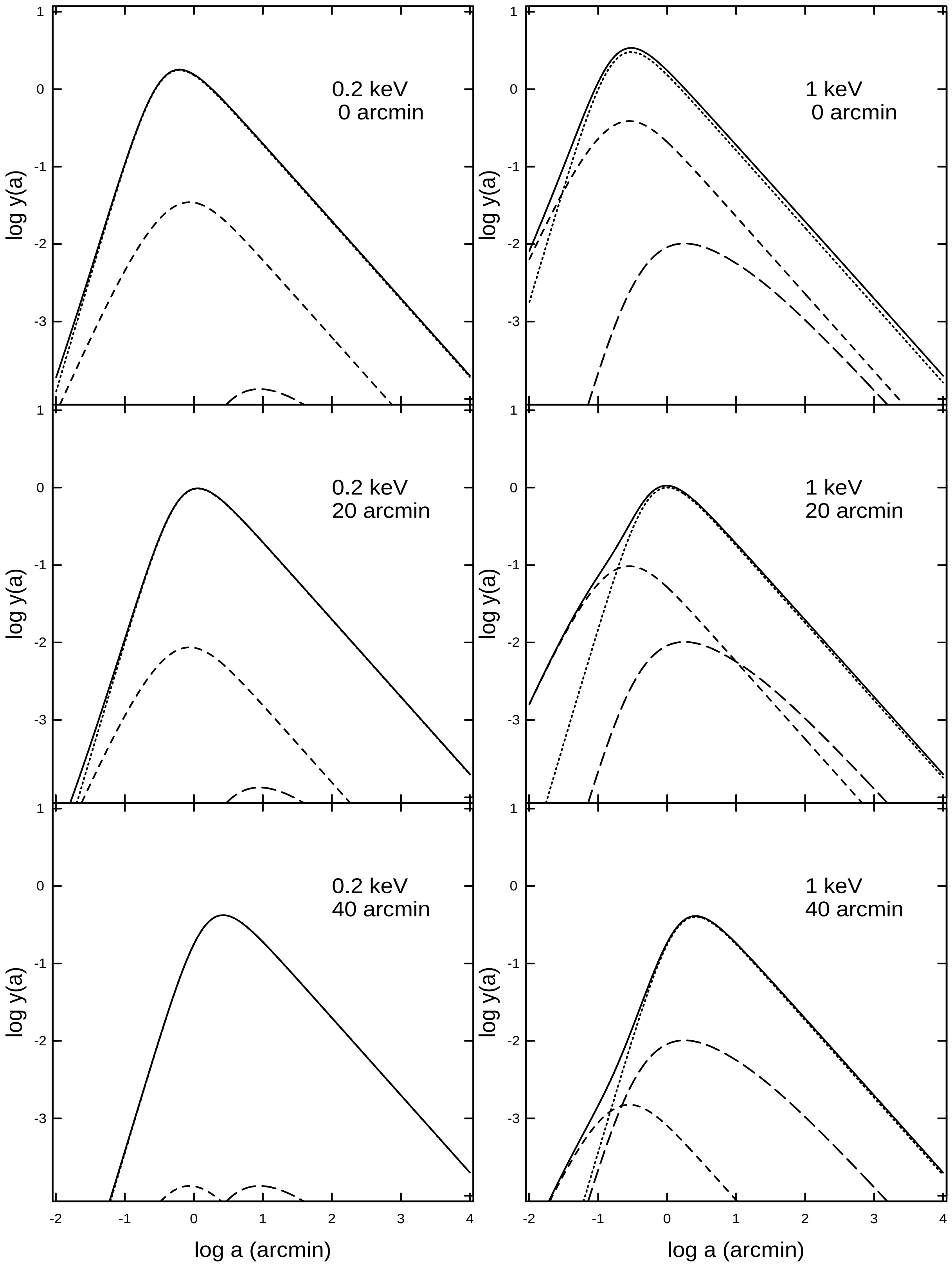

Fig. 15.— Plot of the function $y(a)$ vs. a for the total PSF and for its components, for various energies E and off-axis angles θ. Plotted are the total PSF (solid), and its components gaussian (dotted), exponential (short-dashed), and lorentzian plus power law (long-dashed), respectively.

Table 1. Comparison among Performances of Various Detection Algorithms

Image	$N^{tot}_{\rm WT}$	$N^{tot}_{\rm MPE}$	$N^{tot}_{\rm WGA}$	$N^{only}_{\rm WT}$	$N^{only}_{\rm MPE}$	$N^{only}_{\rm WGA}$	$N_{\rm WT\cap MPE}$	$N_{\rm WT\cap WGA}$	$N_{\rm WGA\cap MPE}$	N_{all}
Full Field of View										
RP200020	36	34	35	7	7	9	26	25	23	22
RP200068	150	100	127	25	6	10	91	114	83	80
RP600008	36	19	27	13	3	6	16	21	14	14
RP600009	80	36	48	39	0	10	34	36	31	29
RP600016	39	41	42	11	14	29	24	10	9	6
RP700028	54	23	50	23	0	21	22	28	20	19
RP701002	58	33	60	16	2	22	31	38	27	27
Total:	453	286	389	134	32	107	244	272	207	197
Off-axis $<$ 25 arcmin										
RP200020	10	12	12	2	5	5	7	7	6	6
RP200068	88	58	76	11	1	5	56	70	50	49
RP600008	20	11	11	8	2	1	9	10	7	7
RP600009	39	18	20	20	1	4	17	16	14	14
RP600016	22	30	8	5	14	7	16	1	0	0
RP700028	33	15	20	16	0	5	14	14	12	11
RP701002	38	19	26	14	2	5	17	21	14	14
Total:	250	163	173	76	25	32	136	139	103	101